Terahertz-frequency InN/GaN heterostructure-barrier varactor diodes

2008 J. Phys.: Condens. Matter 20 384202

(http://iopscience.iop.org/0953-8984/20/38/384202)

J. Phys.: Condens. Matter **20** (2008) 384202 (5pp) doi:10.1088/0953-8984/20/38/384202

Terahertz-frequency InN/GaN heterostructure-barrier varactor diodes

A Reklaitis

Semiconductor Physics Institute, A Goshtauto 11, Vilnius 01108, Lithuania

E-mail: reklaitis@pfi.lt

Received 6 March 2008, in final form 13 May 2008
Published 21 August 2008
Online at stacks.iop.org/JPhysCM/20/384202

Abstract

Frequency multipliers based on the single-barrier and double-barrier InN/GaN heterostructure varactor diodes are suggested. The DC and large-signal AC vertical electron transport in the InN/GaN diodes are investigated by ensemble Monte Carlo simulations. It is found that InN/GaN heterostructure-barrier varactor diodes are able to operate as efficient frequency multipliers in the frequency range up to 1 THz.

1. Introduction

Sources of microwave radiation in the near-terahertz-frequency range can be developed by multiplying the frequency of millimeter waves emitted by conventional solid-state devices (Gunn diodes, avalanche transit-time diodes). Heterostructure-barrier varactor (HBV) diodes have been extensively designed and investigated during the recent years for efficient frequency multiplication [1–6]. A single-barrier HBV diode consists of a thin layer of a large bandgap semiconductor material (the barrier) and thick cladding (modulation) layers of a smaller bandgap material on the two sides of the barrier. Traditional HBV devices are based on the InGaAs/InAlAs and GaAs/AlGaAs material systems. HBV diodes, which are based on the InGaAs/InAlAs and GaAs/AlGaAs material systems, have a symmetric capacitance–voltage (C–V) characteristic about zero bias voltage. This property suppresses the generation of even harmonics, which simplifies the development of high-order harmonic multipliers. An efficiency up to 10% of frequency tripling is obtained experimentally [3] from InGaAs/InAlAs HBV diodes.

At low excitation frequencies, the current response to the input signal is determined by the steady-state C–V characteristic of the HBV diode. The response of the electron distribution in real and momentum space is stationary in this frequency range, i.e., the electron distribution is close to a steady-state during the AC period. The efficiency of frequency multiplication is determined by the modulation ratio $C_{\max}/C_{\min}$, where $C_{\max}$ and $C_{\min}$ are the maximum and minimum capacitance, respectively. Contrary to that, at high excitation frequencies, the operation of HBV diodes is limited by the inertia of electron redistribution [7]. The deterioration of the performance of HBV diodes at high frequencies is caused by the delay of electron redistribution in the modulation layers during the AC period. The strong AC electric field originates in the modulation layers due to the delayed electron redistribution. The strong AC electric field induces electron heating in the modulation layers [8], which results in thermionic emission over the barrier. This is the main reason for the degradation of the device performance for high frequency input signals. For HBV diodes based on the InGaAs/InAlAs and GaAs/AlGaAs material systems, the upper frequency limit of the input signal does not exceed 100 GHz, i.e., the frequency of output signal does not exceed 0.3 THz.

The InN/GaN material system has several serious advantages for the development of the HBV diodes operating in a high-frequency range. First, the rate of the optical phonon emission in InN is 2.5×10^{13} s^{-1}, and it exceeds the emission rate in InGaAs and in GaAs by about four times. Due to a strong electron–phonon coupling, the electron heating in the InN modulation layers originates at much higher frequencies as compared to GaAs and InGaAs. Second, the peak value of the steady-state electron drift velocity in InN reaches 5×10^7 cm s^{-1} [9, 10], and it exceeds the peak drift velocity in GaAs and in InGaAs by about two times. Therefore, the inertia of electron redistribution during the AC period is significantly reduced in InN cladding layers. At high excitation frequencies, the electron response becomes non-stationary, and transient effects come into play. The overshoot of the transient drift velocity in InN exceeds 10^8 cm s^{-1} [9, 11], and it is substantially above the velocity overshoot in GaAs [12] and in InGaAs [13]. Third, the large conduction band offset in InN/GaN heterojunction ensures perfect blocking of the conduction current over the barriers.

In this work, single-barrier and double-barrier InN/GaN HBV diodes are suggested and investigated for frequency

Table 1. Parameters of conduction band structure of wurtzite InN and GaN.

InN			
Valley location	Γ_1	Γ_3	L–M
Number of equivalent valleys	1	1	6
Effective mass	0.04	0.25	1
Intervalley energy separation (eV)	0.0	1.77	2.77
Nonparabolicity parameter (eV^{-1})	1.43	0.0	0.0
Energy gap (eV)	0.7	2.47	3.47
GaN			
Valley location	Γ_1	Γ_3	L–M
Number of equivalent valleys	1	1	6
Effective mass	0.21	1	1
Intervalley energy separation (eV)	0.0	1.9	2.1
Nonparabolicity parameter (eV^{-1})	0.189	0.0	0.0
Energy gap (eV)	3.39	5.29	5.49

tripling into the terahertz-frequency range. The simulations of the vertical electron transport are performed by the ensemble Monte Carlo method self-consistently coupled with the Poisson equation [7, 14]. The calculated DC and large-signal AC characteristics of the InN/GaN HBV diodes show that the diodes may operate in the frequency range of up to 1 THz.

2. Model

Several structures of the single-barrier InN/GaN varactor diode have been investigated for the best performance. The optimized structure is composed of five layers: (1) n-doped InN (200 nm, $N_d = 2 \times 10^{17}$ cm^{-3}); (2) undoped InN (5 nm); (3) undoped GaN (5 nm); (4) a repeat of (2); and finally, (5) a repeat of (1). The structure is sandwiched between two n-type InN contacts doped to 2×10^{19} cm^{-3}.

The details of the Monte Carlo method used in the present work are described in [7]. The conduction band models of InN and GaN consisting of three nonparabolic valleys are taken in the simulations of vertical electron transport in InN/GaN heterostructures. The valleys are represented by spherical dispersion relationships. The minima of the conduction bands are located at the center of the Brillouin zone (Γ_1 point). In wurtzite InN and GaN, the higher valleys of the conduction bands are located at Γ_3 point and at L–M points. The numerical values of the conduction band structure parameters of the wurtzite InN and GaN are taken from [15–17] and summarized in table 1.

The electron scattering mechanisms considered in the simulations include polar optical, deformation acoustic, piezoelectric, intervalley, and ionized impurity scattering. The material parameters for electron scattering in InN and GaN are taken from [16–18]. In the simulations, the electron–electron scattering and Pauli exclusion principle are considered following [19]. Heterojunctions are treated as abrupt interfaces. Electron tunneling and thermionic emission through the heterointerfaces are taken into account. The triangular and trapezoidal shapes of potential barriers are considered for electron tunneling according to the energy of the impinging electron: trapezoidal for the low-energy values and triangular for the high-energy values, respectively. Transmission probabilities for tunneling through the triangular and trapezoidal barriers, which take into account the electron effective mass discontinuity at the heterointerfaces [7], are used in the model. The transmission probabilities are evaluated self-consistently with the instant potential profile. The value for polarization charges at InN/GaN heterointerfaces is estimated from the experimental data of [20, 21]. The InN/GaN conduction band offset is taken from the experimental results of [22]. Table 2 summarizes the material parameters of wurtzite InN and GaN used in the present simulations.

Table 2. Material parameters of wurtzite InN and GaN.

Parameter	InN	GaN
Density (g cm^{-3})	6.81	6.15
Sound velocity (105 cm s^{-1})	3.78	6.56
Acoustic deformation potential (eV)	7.1	8.3
Static dielectric constant	15.3	8.9
High-frequency dielectric constant	8.4	5.35
Polar optical phonon energy (meV)	73	92
Intervalley phonon energy (meV)	73	92
Intervalley deformation potential (109 eV cm^{-1})	1	1
Piezoelectric constant (C cm^{-2})	3.75	3.75
InN/GaN polarization charge density e cm^{-2}	10^{13}	10^{13}
Conduction band offset relative to InN (eV)	—	1.68

When piezoelectric scattering is disregarded, the low-field electron mobility $\mu = 15\,000$ cm^2 V^{-1} s^{-1} in pure bulk InN is obtained at room temperature using the set of material parameters presented in tables 1 and 2. This value of mobility is in agreement with the results of calculations obtained in [17]. Our calculations show that electron mobility in pure InN is reduced to 9800 cm^2 V^{-1} s^{-1} when piezoelectric scattering is taken into account. The electron mobility is further reduced to 2700 cm^2 V^{-1} s^{-1} when ionized impurity scattering at a donor concentration of 4×10^{17} cm^{-3} is considered. This value of electron mobility is in agreement with $\mu = 2100$ cm^2 V^{-1} s^{-1} which is experimentally obtained in [23] at an electron concentration of 3.7×10^{17} cm^{-3}.

It is assumed in the simulations that electrons are at equilibrium with the lattice in the contacts. The electrons are injected from both contacts with a Fermi–Dirac distribution. The electron injection rate dn/dt from each contact is given by

$$\frac{dn}{dt} = n^+ \sqrt{\frac{k_B T}{8m^*}} \frac{\Phi_1(E_F/k_B T)}{\Phi_{1/2}(E_F/k_B T)}, \qquad (1)$$

where n^+ is the electron density in the contact, k_B is the Boltzmann constant, T is the lattice temperature, m^* is the electron effective mass, Φ_1 and $\Phi_{1/2}$ are the Fermi integrals of the order 1 and 1/2, respectively, and E_F is the Fermi energy. The Fermi energy in the contacts is obtained from the numerical solution of the equation $n^+ = 2[2\pi m k_B T/(2\pi\hbar)^2]^{3/2}\Phi_{1/2}(E_F/k_B T)$. The components of the wavevector of each injected electron are selected as random quantities, which satisfy the Fermi–Dirac distribution function.

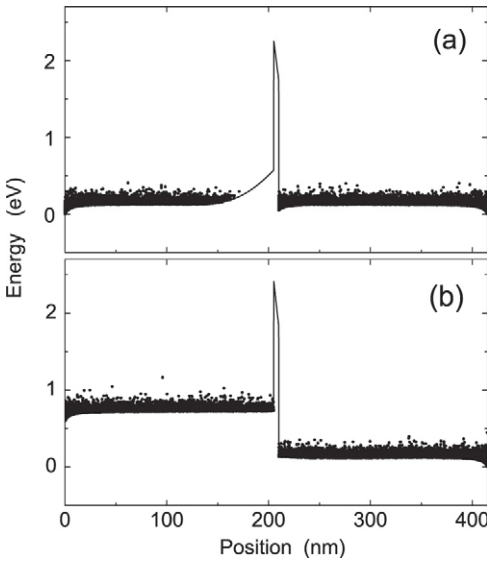

Figure 1. Steady-state profile of the conduction band edge (solid curves) and the distribution of electron kinetic energy (points) in the InN/GaN single-barrier varactor diode. (a) $U = 0$ V (equilibrium distribution). (b) $U = 0.6$ V.

The current density is evaluated in accordance with Shockley–Ramo theorem as [24]

$$j(t) = \frac{\sigma}{L}\sum_{i=1}^{N} v_z(\mathbf{k}_i), \tag{2}$$

where σ is the sheet density of particle charge, L is the thickness of the diode, N is the number of particles, $v_z(\mathbf{k}_i)$ is the instant velocity of the particle in z direction, and $\mathbf{k}_i$ is the wavevector of the ith particle. The C–V characteristic of the structure is obtained from the current response to the ramp of bias voltage. The response of the current density $j(t)$ to the slowly varying bias voltage $U(t)$ can be expressed as

$$j(t) = j_0(U) + C(U)\frac{\mathrm{d}U}{\mathrm{d}t}, \tag{3}$$

where $j_0(U)$ is the steady-state current density, and $C(U)$ is the capacitance per unit area caused by the space charge displacement in the structure. The steady-state current–voltage (I–V) characteristic and the current response to the ramp of bias voltage are evaluated from equation (2) which is valid for the steady-state as well as for the time-dependent transport. The C–V characteristic is evaluated from equation (3). The rate $\mathrm{d}U/\mathrm{d}t$ of the increase in bias voltage is taken sufficiently low to ensure stationary electron distribution in real and momentum space during the simulation of the current response.

To study the large-signal AC diode operation at a given excitation frequency, a diode is driven with a sinusoidal bias voltage. Fourier analysis of the current determines the delivered amplitudes of harmonics.

3. Results and discussion

The potential profile and the electron distribution in the symmetric single-barrier InN/GaN HBV diode are shown in figure 1. The equilibrium potential profile and electron distribution are strongly asymmetric at zero bias voltage due to polarization charges at the heterointerfaces. At equilibrium, the polarization charges at InN/GaN interfaces induce an electric field of about 1.2 MV cm^{-1} in the barrier. The positive polarization at the InN/GaN interface is partially compensated by the accumulated electrons, whereas the negative polarization at the other side of the barrier contributes to the depletion of the InN layer. The polarization charges induce a decrease in the energy difference between the Fermi level and the top of valence band at the negatively polarized heterointerface [25]. The calculations show that for a thicker GaN barrier ($L_b > 7$ nm), the top of the valence band is above the Fermi level, resulting in the formation of accumulated holes in the modulation layer at the InN/GaN interface. At the bias voltage $U = 0.6$ V, the polarization charges at InN/GaN interfaces are completely screened by the accumulated electrons, and the capacitance reaches its maximum value. The results of Monte Carlo simulations show that the tunneling current controls the electron transport in the diode for bias voltages below 5 V. A thermionic current over the barrier was not observed in this range of bias voltage.

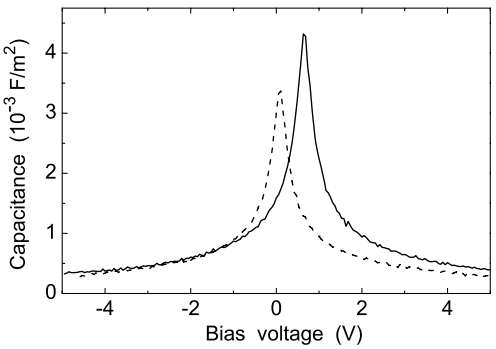

Figure 2. Calculated C–V characteristic of the InN/GaN single-barrier varactor diode (solid curve). The C–V characteristic of the single-barrier $In_{0.53}Ga_{0.47}As$/AlAs varactor diode [7] is shown by the dashed curve for comparison.

The calculated C–V characteristic of the InN/GaN HBV diode is presented in figure 2. The C–V relationship is nearly symmetric with respect to nonzero bias voltage $U_0 = 0.6$ V. The C–V characteristic has an excellent modulation ratio $C_{max}/C_{min} \approx 10$. The high modulation ratio implies that InN/GaN HBV diodes may operate as very efficient frequency multipliers. The results of calculations show that the polarization charges induce a shift of the C–V characteristic without a substantial change of its shape. The shift voltage U_0 of the symmetry point of the C–V characteristic is given by [25]

$$U_0 = \frac{L_b\sigma_p}{\varepsilon\varepsilon_0}, \tag{4}$$

where L_b is the thickness of the barrier, σ_p is the sheet density of polarization charges, and ε and ε_0 are the permittivity and static dielectric constant, respectively. Substituting the following numerical values: $L_b = 5$ nm, $\sigma_p/e = 10^{13}$ cm^{-2}, and $\varepsilon_0 = 15.3$, we obtain $U_0 = 0.59$ V, which is in close agreement with $U_0 = 0.6$ V obtained from Monte Carlo

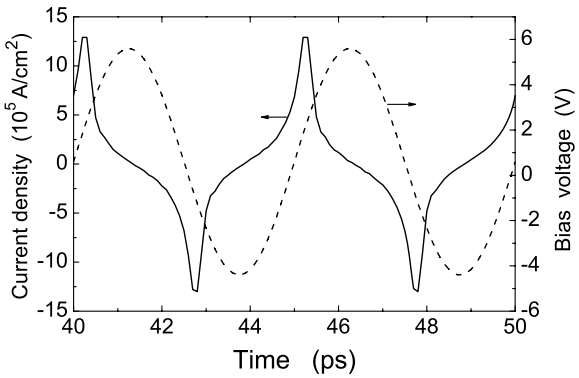

Figure 3. Current response (solid curve) in the InN/GaN single-barrier diode to a sinusoidal excitation of 200 GHz frequency and 5 V amplitude (dashed curve). The DC bias voltage is 0.6 V.

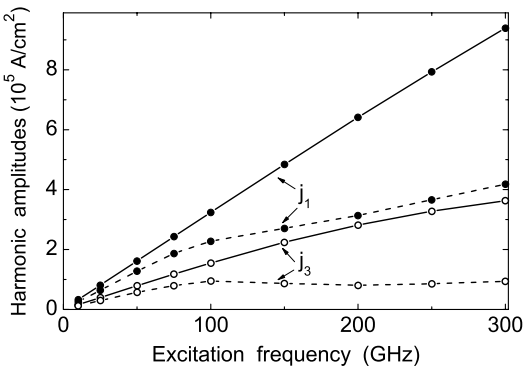

Figure 4. First (j_1) and third (j_3) harmonic amplitudes of the current oscillations versus excitation frequency in InN/GaN single-barrier varactor diode (solid curves). The amplitude of the sinusoidal excitation is 5 V, and the DC bias voltage is 0.6 V. The dashed curves show the corresponding harmonic amplitudes of the current response in $In_{0.53}Ga_{0.47}As$/AlAs single-barrier varactor diode [7].

simulations. The comparison of the C–V relationships of InN/GaN and $In_{0.53}Ga_{0.47}As$/AlAs varactor diodes (figure 2) shows that the InN/GaN material system is more suitable for frequency multiplication at low excitation frequencies at which the inertia of electron redistribution is not manifested.

The calculated response of the current $j(t)$ to the sinusoidal excitation voltage (figure 3) shows that the current follows the steady-state C–V relationship even though the excitation frequency is 200 GHz. The inertia of electron redistribution in the modulation layers is not manifested during the AC period in the frequency range below 200 GHz due to high electron velocity and fast phonon emission.

This fact is confirmed by the calculated amplitudes of the first and third harmonics (figure 4). In the low-frequency range, the amplitude j_n of the nth harmonic is directly proportional to the excitation frequency f as

$$j_n = 2\pi f U_1 \int_0^{2\pi} C(U_0 + U_1 \sin\omega) \cos n\omega \, \mathrm{d}\omega, \qquad (5)$$

where $C(U_0 + U_1 \sin\omega)$ is the steady-state C–V characteristic of the diode, and U_1 is the amplitude of the excitation. As seen from figure 4, the third harmonic amplitude j_3 generated by the InN/GaN diode exhibits a near-linear dependence on excitation frequency even beyond 200 GHz. Contrary to that, j_3 generated by the $In_{0.53}Ga_{0.47}As$/AlAs diode tends to decrease in the frequency range above 100 GHz. An additional point to emphasize is that the ratio j_3/j_1 of the harmonic amplitudes generated by the InN/GaN diode is significantly higher as compared to the corresponding ratio obtained from the $In_{0.53}Ga_{0.47}As$//AlAs diode. At low excitation frequencies, the enhanced performance of the InN/GaN diode is caused by the larger modulation ratio C_{max}/C_{min} of the steady-state C–V characteristic of the InN/GaN diode as compared to the $In_{0.53}Ga_{0.47}As$/AlAs diode (figure 2). In the high-frequency range, the significantly less pronounced inertia of electron redistribution in the modulation layers is responsible for the enhanced performance of the InN/GaN diode. It is seen from the results presented in figure 4 that the InN/GaN HBV diode is able to operate as an efficient frequency tripler in the 1 THz frequency band.

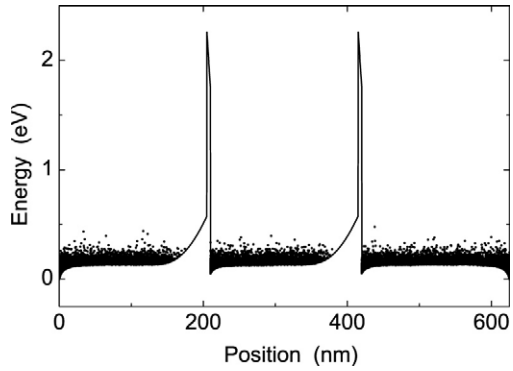

Figure 5. Equilibrium profile of the conduction band edge (solid curve) and the distribution of electron kinetic energy (points) in the double-barrier InN/GaN varactor diode.

The development of multibarrier HBV diodes [2, 3, 6] makes it possible to improve the characteristics of the frequency multipliers. The improved characteristics of the multibarrier HBV diodes include increased diode impedance and higher power handling capability [6]. In order to investigate the multibarrier InN/GaN varactor diode, the double-barrier diode based on the InN/GaN material system is simulated in the present work. The simulated double-barrier structure consists of nine layers: (1) n-InN (200 nm, $N_d = 2 \times 10^{17}$ cm^{-3}); (2) undoped InN (5 nm); (3) undoped GaN (5 nm); (4) a repeat of (2); (5) a repeat of (1); (6) a repeat of (2); (7) a repeat of (3); (8) a repeat of (2); and finally, (9) a repeat of (1). The structure is sandwiched between n-InN contacts doped to 2×10^{19} cm^{-3}.

The equilibrium band edge profile and the electron distribution in the double-barrier diode are presented in figure 5. The calculated C–V characteristic of the diode is shown in figure 6. The symmetry point of the C–V characteristic is shifted to a bias voltage $U_0 = 1.2$ V, which is twice that for the single-barrier diode. The peak value of the diode capacitance C_{max} is reduced to half the value of the single-barrier diode. This reduction is consistent with the

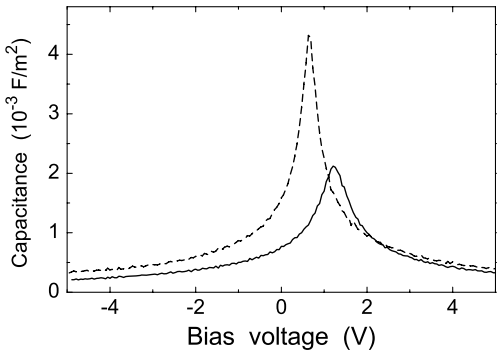

Figure 6. A comparison of the C–V characteristics of the double-barrier (solid curve) and the single-barrier (dashed curve) InN/GaN varactor diodes.

treatment of the double-barrier diode as the two single-barrier capacitors connected in series. However, the double reduction in the minimum capacitance $C_{\min}$ was not obtained from the simulations (figure 6). As a result, the modulation ratio of the C–V characteristic of the double-barrier diode $C_{\max}/C_{\min} \approx 6$ is lower as compared to the single-barrier diode.

The interfaces of InN/GaN heterostructures are known to be rough interfaces having a fairly large deviation from the perfect planes. To investigate the influence of heterointerface roughness on the properties of vertical electron transport in InN/GaN HBV diodes, the single-barrier HBV diode is simulated by taking into account the reflection of electrons from the rough heterointerfaces. The reflection from the rough interfaces is considered classically. To this end, the specular electron reflection from the heterojunction barrier is replaced by the diffuse electron reflection [26]. In the model of specular reflection, the normal to heterointerface wavevector component k_z of the incident electron is changed to $-k_z$ in the reflection event. In the diffuse model, the direction of the wavevector of the reflected electron is selected randomly from an isotropic distribution on semi-sphere with the main axis in the direction $-k_z$. The modulus of the wavevector is conserved in the diffuse reflection event. The results of the calculations of the C–V characteristics show that both models give the same results within an accuracy of 5 per cent, which is limited by the statistical errors. The minor effect of the interface roughness on the C–V characteristic can be explained by the diffusive nature of electron motion in the modulation InN layers. The reflected electrons rapidly lose their direction of motion due to intensive phonon and impurity scattering.

4. Conclusions

Single-barrier and double-barrier InN/GaN varactor diodes are proposed for efficient frequency multiplication. The electron transport in the diodes is investigated by Monte Carlo simulations. It is found that the polarization charges at InN/GaN interfaces induce a shift of the symmetric C–V characteristic of the diodes. The results of the simulations show that InN/GaN varactor diodes are able to operate as efficient frequency triplers in 1 THz frequency range.

Acknowledgments

The work was supported by the Lithuanian State Science and Studies Foundation under contract C-07004.

References

[1] Kollberg E and Rydberg A 1989 *Electron. Lett.* **25** 1696
[2] Jones J R, Bishop W L, Jones S H and Tait G B 1997 *IEEE Trans. Electron Devices* **45** 512
[3] Melique X, Maestrini A, Farre R, Mounaix P, Favreau M, Vanbesien O, Goutoule J-M, Mollot F, Beaudin G, Närhi T and Lippens D 2000 *IEEE Trans. Electron Devices* **48** 1000
[4] Stake J, Jones S H, Dillner L, Hollung S and Kollberg E L 2000 *IEEE Trans. Microw. Theory Tech.* **48** 677
[5] Saglam M, Mutamba K, Megej A, Sydlo C and Hartnagel H L 2003 *Appl. Phys. Lett.* **82** 227
[6] Emadi T A, Bryllert T, Sadeghi M, Vukusic J and Stake J 2007 *Appl. Phys. Lett.* **90** 012108
[7] Reklaitis A and Grigaliūnaitė G 2001 *Phys. Rev.* B **63** 155301
[8] Pozhela Y and Reklaitis A 1979 *Fiz. Tekh. Poluprovodn.* **13** 1127
Pozhela Y and Reklaitis A 1979 *Sov. Phys. Semicond.* **13** 660
[9] Tsen K T, Poweleit C, Ferry D K, Lu H and Schaff W J 2005 *Appl. Phys. Lett.* **86** 222103
[10] Liang L W, Tsen K T, Poweleit C, Ferry D K, Tsen S-W D, Lu H and Schaff W J 2005 *Phys. Status Solidi* c **2** 2297
[11] O'Leary S K, Foutz B E, Shur M S and Eastman L F 2005 *Appl. Phys. Lett.* **87** 222103
[12] Matulionis A, Požela J and Reklaitis A 1976 *Phys. Status Solidi* a **35** 43
[13] Nag B R, Ahmed S R and Deb Roy M 1986 *IEEE Trans. Electron Devices* **33** 788
[14] Ryzhii M, Ryzhii V, Suris R and Hamaguchi C 2000 *Phys. Rev.* B **61** 2742
[15] Fritsch D, Schmidt H and Grundmann M 2004 *Phys. Rev.* B **69** 165204
[16] Foutz B E, O'Leary S K, Shur M S and Eastman L F 1999 *J. Appl. Phys.* **85** 7727
[17] Polyakov V M and Schwierz F 2006 *Appl. Phys. Lett.* **88** 032101
[18] O'Leary S K, Foutz B E, Shur M S and Eastman L F 2006 *J. Mater. Sci., Mater. Electron.* **17** 87
[19] Reklaitis A 2006 *Phys. Rev.* B **74** 165305
[20] Zhang H, Miller E J, Yu E T, Poblenz C and Speck J S 2004 *Appl. Phys. Lett.* **84** 4644
[21] Veal T D, Piper L F J, Mahboob I, Lu H, Schaff W J and McConville C F 2005 *Phys. Status Solidi* c **2** 2246
[22] Wang K A, Lian C, Su N, Jena D and Timler J 2007 *Appl. Phys. Lett.* **91** 232117
[23] Chen F, Cartwright A N, Lu H and Schaff W J 2005 *Appl. Phys. Lett.* **87** 212104
[24] Junevičius D and Reklaitis A 1988 *Electron. Lett.* **24** 1307
[25] Reklaitis A 2005 *Appl. Phys. Lett.* **86** 262110
[26] Ando T, Fowler A B and Stern F 1982 *Rev. Mod. Phys.* **54** 437